# Multifunctional Compounds for Activation of the p53-Y220C Mutant in Cancer

Jessica J. Miller,[a] Christophe Orvain,[b] Shireen Jozi,[a] Ryan M. Clarke,[a] Jason R. Smith,[a] Anaïs Blanchet,[b] Christian Gaiddon,*[b] Jeffrey J. Warren,*[a] and Tim Storr*[a]

**Abstract:** The p53 protein plays a major role in cancer prevention, and over 50% of cancer diagnoses can be attributed to p53 malfunction. The common p53 mutation Y220C causes local protein unfolding, aggregation, and can result in a loss of Zn in the DNA-binding domain. Structural analysis has shown that this mutant creates a surface site that can be stabilized using small molecules, and herein a multifunctional approach to restore function to p53-Y220C is reported. A series of compounds has been designed that contain iodinated phenols aimed for interaction and stabilization of the p53-Y220C surface cavity, and Zn-binding fragments for metallochaperone activity. Their Zn-binding affinity was characterized using spectroscopic methods and demonstrate the ability of compounds **L4** and **L5** to increase intracellular levels of $Zn^{2+}$ in a p53-Y220C-mutant cell line. The in vitro cytotoxicity of our compounds was initially screened by the National Cancer Institute (NCI-60), followed by testing in three stomach cancer cell lines with varying p53 status', including AGS (WTp53), MKN1 (V143A), and NUGC3 (Y220C). Our most promising ligand, **L5**, is nearly 3-fold more cytotoxic than cisplatin in a large number of cell lines. The impressive cytotoxicity of **L5** is further maintained in a NUGC3 3D spheroid model. **L5** also induces Y220C-specific apoptosis in a cleaved caspase-3 assay, reduces levels of unfolded mutant p53, and recovers p53 transcriptional function in the NUGC3 cell line. These results show that these multifunctional scaffolds have the potential to restore wild-type function in mutant p53-Y220C.

## Introduction

The p53 protein, referred to as the "guardian of the human genome,"[1] is a tetrameric transcription factor that regulates the expression of target genes to induce antiproliferative cellular responses.[2] Among those genes are those that initiate apoptosis, DNA repair, and cell cycle arrest of damaged cells.[3] However, in over 50% of cancer diagnoses, p53 does not carry out its essential function.[4] The most common alterations to p53 are point mutations that affect tertiary structure or alter the protein's ability to bind DNA.[5] The net result is that cells bearing malfunctioning p53 are susceptible to enhanced proliferation and survival.[6] There is significant therapeutic potential for p53, and pharmacological restoration of function to mutant p53 is an acknowledged chemotherapeutic target.[7] Herein, we describe the synthesis, characterization, and in vitro testing of a new series of bifunctional ligands designed to restore function in mutant p53, specifically the Y220C point mutation.

The majority of p53 mutations are point mutations localized to the protein's core DNA-binding (p53C) domain,[6] and a number of small molecules have been developed in an effort to reactivate mutant p53.[8] One such example is APR-246 (Scheme 1a), which has shown positive results in a Phase I/II clinical trial.[9] APR-246 is a pro-drug and is activated to a Michael acceptor that binds covalently to cysteine residues of

[a] J. J. Miller, S. Jozi, R. M. Clarke, J. R. Smith, Prof. J. J. Warren, Prof. T. Storr
Department of Chemistry
Simon Fraser University
8888 University Drive
Burnaby (Canada)
E-mail: j_warren@sfu.ca
      tim_storr@sfu.ca

[b] C. Orvain, A. Blanchet, C. Gaiddon
Inserm UMR_S 1113
Molecular Mechanisms of Stress Response and Pathologies
Université de Strasbourg
Strasbourg (France)
E-mail: gaiddon@unistra.fr

Supporting information and the ORCID identification number(s) for the author(s) of this article can be found under:
https://doi.org/10.1002/chem.201802677.
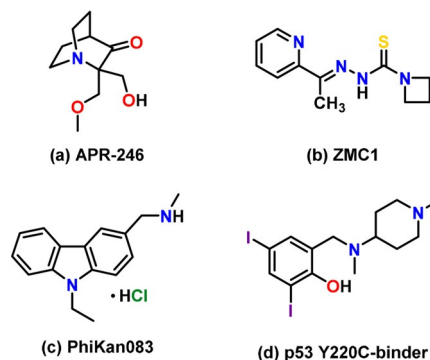


**Scheme 1.** Chemical structures of (a) APR-246 (PRIMA-1MET) (b) NSC319726 (ZMC1) (c) PhiKan083 and (d) iodinated phenol small molecule shown to bind the p53 Y220C mutant pocket.

mutant p53, resulting in protein reactivation.[10] Due to the non-specific nature of this process, APR-246 also binds other proteins, and modification of thioredoxin reductase 1 leads to increased reactive oxygen species (ROS) production, an additional cytotoxic mechanism.[11]

The p53C domain contains a single $Zn^{2+}$ ion that is required for proper protein folding and function.[12] Mutations to p53C can disrupt protein stability and/or cause loss of Zn.[13] Consequently, the discovery of small molecule Zn chaperones aimed to restore wild-type function in mutant p53 has generated much attention.[8c, 14] For example, the thiosemicarbazone ligand ZMC1 (Scheme 1b) induces conformational "wild-type-like" change in the common Zn-binding p53 mutation (R175H), and restores p53 transactivation function.[14] Further studies indicate that subtle tuning of the Zn-binding affinity of the metallochaperones is critical for p53 reactivation,[15] as it functions by repopulating Zn-deficient p53C with $Zn^{2+}$.[16] More broadly, targeted metal ion chelation and redistribution has been shown as a promising anti-cancer strategy,[17] and a number of recent studies have highlighted both the novelty and complexity of this approach.[8c, 18]

Mutations to the p53C domain can result in structural destabilization such that the protein unfolds at or below physiological temperatures.[3a] The Y220C point mutation is a common destabilizing p53 mutation and contributes to about 75 000 new cancer cases each year.[8b] It results in a cavity at the surface of the protein, which decreases the melting point of the protein by around 2 °C and contributes to unfolding and ultimately aggregation.[3a] Small molecules that bind to the Y220C cavity were developed using in silico and in vitro screening, and the carbazole-based molecule PhiKan083 (Scheme 1c) was identified to raise the melting temperature ($T_m$) and slow the rate of thermal denaturation of p53-Y220C.[19] More recently, derivatives of halogenated phenols have been reported by Boeckler and co-workers as a class of molecules that bind to the p53-Y220C cavity (Scheme 1d).[8b] It is hypothesized that halogen-bonding interactions with amino acids inside the cavity plays an important role in binding. The halogenated compounds modestly increase the melting temperature of a p53-Y220C model protein and slow the rate of thermally induced protein unfolding/aggregation.[8b] These results demonstrate that an iodinated-phenol core can be a starting point for envisioning new molecular designs. In addition to protein unfolding, p53 Y220C is prone to the loss of $Zn^{2+}$ in the DNA-binding domain,[12, 13, 20] presenting a new opportunity for drug design.

Multifunctional drugs, namely agents with more than one therapeutic mechanism, have gained increasing acceptance in recent years.[21] Multifunctional drugs offer potential advantages over their monofunctional counterparts, namely the potential to produce additive or synergistic effects by acting on multiple targets or designing one component to enhance druggable characteristics of the therapeutic molecule such as blood–brain-barrier penetration or tissue specificity.[22] Such characteristics have been successful at enhancing drug efficacy and lowering toxic side effects, providing a new avenue in drug discovery from a "one-drug-one-target" to a "one-drug-multiple-target" strategy.[21d, 23] Herein, we report a new series of bifunctional ligands designed to restore wild-type activity in p53-Y220C by serving as structural stabilizers and as Zn-chaperones. Our new series of compounds feature different binding groups that tune $Zn^{2+}$ affinities and promote interactions with p53-Y220C.

## Results and Discussion

### Ligand design and synthesis

A series of ligands (L1-L5) that are designed to restore wild-type function in p53-Y220C were synthesized and characterized (Scheme 2). The ligand series was designed with two
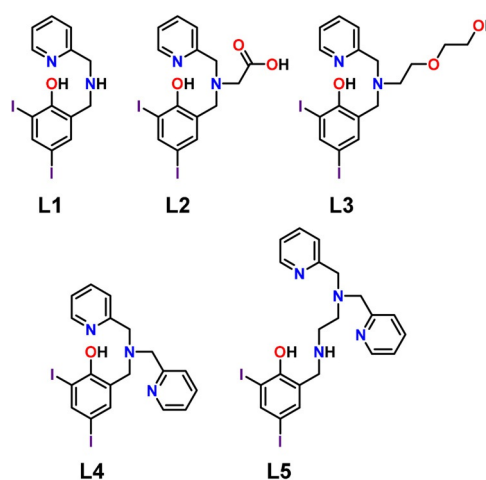


**Scheme 2.** Chemical structure of ligands **L1**–**L5**.

motifs in mind: (1) a p53-Y220C binding diiodophenol core,[8b] and (2) Zn-binding groups to promote metallochaperone activity.[8c, 16, 24] Metal-binding groups were installed at the 2-position, following rationales for related p53-binding molecules.[8b] Complexes of **L1** with a number of different metal ions have been investigated for their anti-cancer activity, however, the neutral metal complexes have low aqueous solubility.[25] The carboxylic acid (**L2**) and polyethylene glycol (**L3**) groups were added to promote water solubility and biological compatibility, respectively. **L4** and **L5** include additional metal-binding groups to promote 1:1 $Zn^{2+}$ to ligand complex formation.

### Molecular docking

To investigate the potential binding mode of **L1**–**L5** with the mutation-induced cavity in p53-Y220C we employed molecular docking of the ligands with available X-ray data.[8b] Our modelling results predict that the iodinated phenol moiety in **L1**–**L5** orients in the p53-Y220C cavity (Figure 1, S12–14) in a similar fashion to a known p53-Y220C ligand that incorporates the same diiodophenol pharmacophore.[8b] In addition, the DPA metal-binding unit in **L4** and **L5** does not significantly alter the interaction, with our lead compound **L5** (vide infra) overlap-
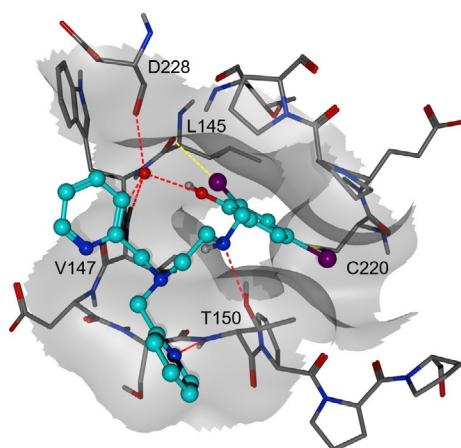
**Figure 1.** A low energy pose of **L5** in the mutation-induced cavity for p53-Y220C (PDBID: 4AGQ).[8b] The halogen bonding interaction (I⋯Leu145) is shown with a yellow line. The hydrogen bond network between the conserved water, D228, and V147 is shown in red. The Van der Waals surface of the protein is shown in gray. Atom colors: carbons represented in gray in the protein and teal for the ligand. Oxygen is shown in red, nitrogen in blue, and sulfur in yellow. Polar hydrogens are shown in white. Non-polar hydrogens are omitted for clarity.

ping with X-ray data (PDBID: 4AGQ) for a known p53-Y220C binding ligand (Figure S11).

## Zinc-binding properties

Previously reported models for Zn-binding in p53 describe two possible ligation sites, the native binding site ($K_{d1}$) and non-native ($K_{d2}$) sites.[26] The native $Zn^{2+}$ $K_{d1}$ for WTp53 is estimated to be on the order of $10^{-12}$ M.[16,27] This value derives from the low intracellular levels of free zinc,[16,27] and the fact that under physiological conditions, WTp53 is predominantly in the holo (zinc-bound) form.[28] Metallochaperones designed to rescue zinc-binding in p53 mutants should therefore have $Zn^{2+}$ affinities that are less than that of the native site ($K_{d1}$), yet higher than that of non-native sites ($K_{d2}$), estimated to be about $10^{-6}$ M for WTp53.[8c] The p53-Y220C mutant is prone to the loss of $Zn^{2+}$ due to local unfolding and increased aggregation, so the exact value of $K_{d1}$ is unknown. Assuming that the p53 Y220C mutant should have a slightly weaker Zn affinity than WTp53, we designed Zn-metallochaperones for p53-Y220C where the Zn affinity is in between $K_{d2}$ and $K_{d1}$ ($10^{-9} < K_d$ chelator $< 10^{-12}$).

Spectrophotometric (UV-visible) pH titrations were carried out to characterize ligand speciation and Zn-affinity for **L1**–**L5**. These studies show that, at biological pH (7.4), both 1:1 and 2:1 ligand:$Zn^{2+}$ complexes are present for **L1**, **L2**, and **L3** (Figure 2).[25] Verani and co-workers proposed that the 1:1 Zn:**L1** species is the biologically active form.[25] Our speciation results are in accord with this observation, predicting that [Zn**L1**]$^+$ is the major constituent in solution at pH 7.4. In contrast, speciation diagrams of ligands **L4** and **L5** are described by a model with only 1:1 ligand to metal species present (Figure 2). This result is consistent with the presence of an additional Zn-binding N-(2-pyridylmethyl) moiety in these li-
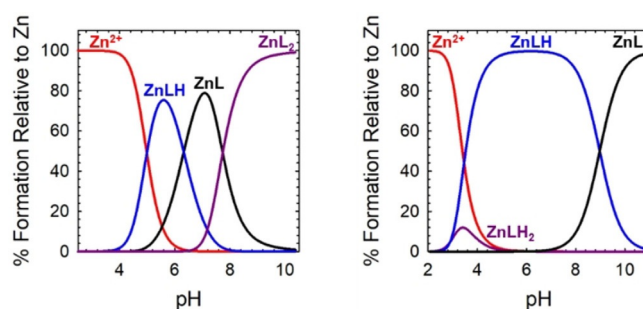


**Figure 2.** (left) Simulated species distribution plot of $Zn^{2+} +$ **L1**. (right) Simulated speciation plot of $Zn^{2+} +$ **L5**. Speciation diagrams made using HySS2009.

gands.[29] Complete data sets, models, and simulations are given in the Supporting Information.

Analysis of the speciation diagrams for each ligand provides the $Zn^{2+}$ affinity of each ligand at physiological pH. The concentration of free $Zn^{2+}$ present in solution at a given pH, referred to as pM (pZn = $-$log[Zn$_{unchelated}$]), is a direct estimate of the metal-ligand affinity when all species in solution are considered.[30] Calculated values for pZn are reported in Table 1.

**Table 1.** Stability constants (log$K$) of the Zn complexes of **L1**–**L5** and calculated pM values[a] (errors are for the last digit).

|  | pZn[a] (pH 7.4) | Log $K$ ZnL | ZnLH | ZnLH$_2$ | ZnL$_2$ |
|---|---|---|---|---|---|
| **L1** | 9.2 | 14.63(1) | 6.327(5) | – | 10.34(5) |
| **L2** | 10.1 | 15.439(6) | 5.572(4) | – | 10.65(4) |
| **L3** | 9.4 | 13.59(1) | 6.427(5) | – | 10.04(3) |
| **L4** | 7.9 | 14.72(1) | 7.802(8) | – | – |
| **L5** | 8.4 | 14.63(3) | 8.98(2) | 2.89(3) | – |

[a] pZn was calculated using pZn = ($-$log[Zn$^{2+}$]$_{free}$), where $Zn^{2+}$ is determined from the Hyss model.[31] [**L1**–**L3**] = 6.25 μM, [**L4**–**L5**] = [Zn$^{2+}$] = 12.5 μM, 25 °C, I = 150 mM NaCl.

The calculated pM values for **L1**–**L3** demonstrate a high $Zn^{2+}$-affinity at physiological pH, however, exhibit limited biological activity (vide infra). The calculated pZn values for the 1:1 complexes **L4** and **L5** are comparable (7.9 and 8.4 respectively), and match well with reported Zn-affinities for a ligand series containing the same metal-binding fragment.[29] These values afford approximate dissociation constants ($K_d$) in the low nanomolar range, an affinity appropriate for functioning as Zn metallochaperones for p53-Y220C.

Zn complexes of **L4** and **L5** were also isolated and characterized using $^1$H NMR, MS, and X-ray crystallography (for Zn**L4**Cl, Figure 3), and are in accord with the 1:1 binding of **L4** and **L5** to $Zn^{2+}$ modelled above for variable pH titrations. Complete crystallographic information is in the Supporting Information (Table S2).
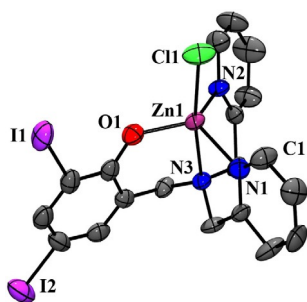
**Figure 3.** ORTEP of Zn**L4**Cl (50% probability) using POV-Ray, excluding hydrogen atoms and solvent. Selected interatomic distances [Å]: Zn(1)–N(1-3): 2.093–2.280; Zn(1)–O(1): 1.954; Zn(1)–Cl(1): 2.286.

## Increasing intracellular levels of $Zn^{2+}$ in the p53 Y220C cell line NUGC3

We investigated whether **L4** and **L5** could serve as Zn-metallo-chaperones and increase intracellular levels of $Zn^{2+}$ in the stomach cancer p53-Y220C cell line NUGC3. NUGC3 cells were incubated with the fluorescent $Zn^{2+}$ sensitive probe FZ3-AM (1 μM),[32] followed by incubation with **L4** or **L5** (15 μM), 50 μM $ZnCl_2$, and subsequent imaging. Pyrithione was used as a positive control for Zn uptake. Both **L4** and **L5** increased intracellular levels of $Zn^{2+}$ in NUGC3 cells, as indicated by increased intracellular fluorescence (Figure 4). However, due to the similar Zn $K_d$ values of FZ3-AM and **L4**/**L5** ($Zn^{2+}$ $K_d = 15$ nM for FZ3-AM,[32] 13 nM for **L4**, and 4 nM for **L5**) Zn-binding to the fluorophore in this experiment is likely restricted, and thus total Zn
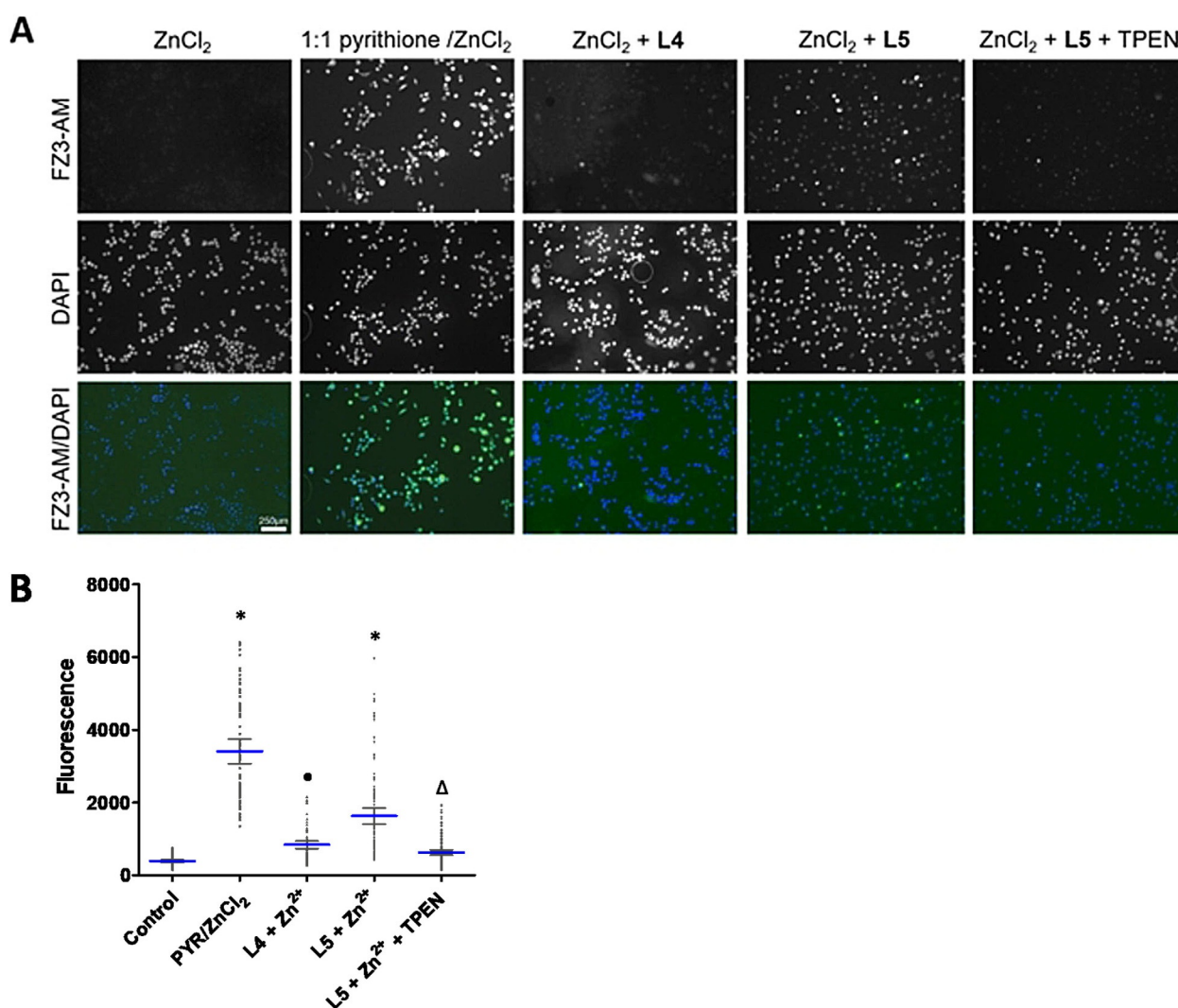


**Figure 4.** Treatment of NUGC3 (p53 Y220C) with **L4** and **L5** increases intracellular $Zn^{2+}$. (a) Imaging of intracellular $Zn^{2+}$ levels in complete serum-free media. NUGC3 cells were incubated with 1 μM FZ3-AM[24] for 20 minutes at 37°C, followed by incubation with indicated treatment ($ZnCl_2 = 50$ μM, **L4** = **L5** = 15 μM, 50 μM PYR) for 2 hours. 150 μM TPEN was added following incubation with $ZnCl_2$ and **L5**. Cells were imaged using a Nikon ApoTome microscope and fluorescence-quantified using ImageJ. All images were taken at indicated magnification. (B) Fluorescence intensity of FZ3-AM at 488 nm demonstrating relative $Zn^{2+}$ levels. Blue line indicates mean values, while black error bars demonstrate the 95% confidence interval. * indicates statistical differences from control with $p < 0.0001$, ● indicates statistical differences from control with $p < 0.01$, and Δ indicates statistical difference from **L5** + $ZnCl_2$ with $p < 0.0001$. No statistical differences are observed between the control and **L5** + $ZnCl_2$ + TPEN.

uptake is underestimated. **L5** increased intracellular $Zn^{2+}$ levels more than 4-fold compared to the untreated control, and a two-fold increase over treatment is observed with **L4** (Figure 4). Addition of the strong membrane-permeable Zn-chelator, *N-N-N′-N′*-tetrakis-(2-picolyl)-ethylenediamine (TPEN, $K_d = 26$ fM)[33] following treatment with **L5** results in a significant loss of fluorescence, indicating the ability of **L5** to deliver intracellular $Zn^{2+}$ to stronger Zn chelates. These results demonstrate the ability of **L5** and to a lesser extent, **L4**, to serve as Zn-metallochaperones in NUGC3 cells containing the p53-Y220C mutation.

## In vitro cytotoxicity assays

**L1**–**L5** and the corresponding zinc complexes of **L4** and **L5** (Zn**L4**Cl and Zn**L5**Cl) were submitted to the National Cancer Institute's NCI-60 program for in vitro screening against a panel of 60 human cancer cell lines. After initial 1-dose screening (10 μM), **L1**–**L3** were rejected from further testing due to their insufficient cytotoxicity (Table S3). The inactivity of these 2:1 $Zn^{2+}$-binding ligands could be due to different factors, including limited cell uptake of the ligands, and/or limited solubility of neutral complexes formed from available $Zn^{2+}$ found in cell culture media.[33] These ligands were not subjected to further testing and will not be discussed further. The activity of the 1:1 $Zn^{2+}$ binding ligands, **L4** and **L5**, was significantly greater and the aggregate results from their 5-dose testing are displayed in Table 2. **L4** and **L5** were found to have a broad range of cyto-

**Table 2.** Mean GI$_{50}$ and LC$_{50}$ values for **L4**, **L5**, and cisplatin from the NCI-60 screen.

| Ligand | NSC Number[a] | GI$_{50}$ [μM][b] | LC$_{50}$ [μM][b] |
|---|---|---|---|
| L4 | 788646 | 2.2 | 70.3 |
| L5 | 788647 | 1.5 | 15.0 |
| Cisplatin | 119875 | 1.5 | 44.0 |

[a] NSC number is the compounds internal ID number at the National Cancer Institute. [b] GI$_{50}$ values correspond to the dose that inhibits 50% of cell growth compared to non-treated controls, while LC$_{50}$ indicates the concentration required to kill 50% of treated cells.[35]

static (GI$_{50}$, 0.4–2.2 μM) and cytotoxic (LC$_{50}$, 4.6–93.8 μM) activity. **L5** shows the most promising results, exhibiting high cytostatic activity in combination with a cytotoxic activity that is almost three times more potent than that of cisplatin. This combination of both cytostatic and cytotoxic activity can offer major advantages in the treatment of cancers.[34]

Interestingly, their corresponding Zn complexes (Zn**L4**Cl and Zn**L5**Cl) exhibited lower biological activity at the initial test concentration of 10 μM (Table S3), and did not meet the necessary threshold for 5-dose testing in the NCI-60 panel. However, further investigation of the Zn complexes using stomach cancer cell lines AGS (WTp53) and NUGC3 (p53-Y220C) showed that their cytotoxicity increases at higher concentrations (Figures S37–S40), with Zn**L4**Cl exhibiting increased cytotoxicity in comparison to **L4** at concentrations >10 μM.

Conversely, **L5** is more cytotoxic than Zn**L5**Cl in both AGS and NUGC3 cell lines at all concentrations studied.

A heat map of the 5-dose NCI-60 screen for **L4** and **L5** is shown in Figure 5, and summarizes the patterns of in vitro cytotoxicity (GI$_{50}$ and LC$_{50}$) from low activity (blue) to high activity (red). The most striking result is the level of cytotoxicity dis-
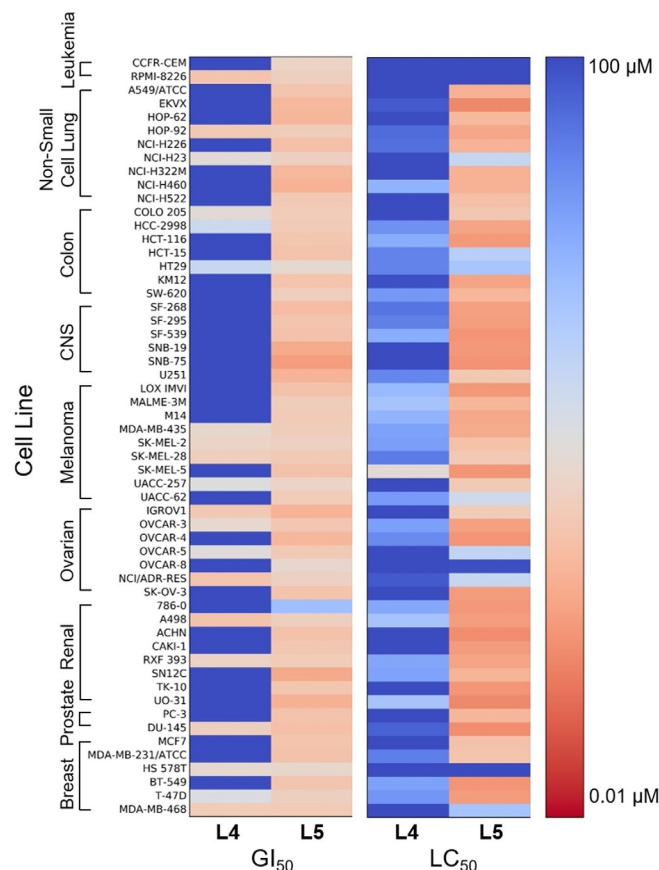


**Figure 5.** Heat map showing the in vitro cytotoxicity (left: $\log_{10}$ GI$_{50}$; right: $\log_{10}$ LC$_{50}$) of **L4** and **L5** in the NCI-60 screen. Blue indicates low cytotoxicity (100 μM) and red indicates high cytotoxicity (0.01 μM).

played by **L5** across most cell lines. However, **L4** and **L5** have little cytotoxic effect on leukemia cell lines (>100 μM in all cases). Chemoresistance in leukemia cancers are common, especially in multiple myeloma (RPMI-8226).[36] In contrast, **L4** and **L5** are highly cytotoxic on the melanoma cell line SK-MEL-5, with GI$_{50}$ values 2.6 and 1.5 μM and LC$_{50}$ values of 13.0 and 5.2 μM, respectively. Note that the NCI-60 panel does not presently contain p53-Y220C mutant cell lines, though many other p53 mutants are included. In addition, several highly lethal cancer types are not represented in the NCI-60 screen (i.e. gastric cancer, pancreatic cancer).

For these two reasons, we further investigated the biological activity of our compounds in gastric cancer cells. Gastric cancer is the second leading cause of cancer-related deaths worldwide, and its lethality is particularly high as indicated by a 5-year survival rate of around 30%.[37] In addition, there are gastric cancer cell lines with different p53 status', including

p53- Y220C. We tested the in vitro cytotoxicity of our ligand series on three human gastric cancer cell lines: AGS, which contains wild-type p53, MKN1, with the V143A point mutation, and NUGC3, which has the p53-Y220C mutant. The data are reported in Table 3 as $IC_{50}$ values. The results are in agreement



**Figure 6.** NUGC3 cells (300 cells/well; 96 wells/plate) were grown for 4 days and then treated for 3 days at $IC_{50}$ and $IC_{75}$ concentrations as indicated. 3D cultures were observed by microscopy to estimate clone size (left) and cell survival was assayed using rezasurin (right). * indicates statistical differences from non-treated control with $p < 0.001$ as established by ANOVA followed by Tukey test.

| Table 3. In vitro cytotoxicity ($IC_{50}$ values)[a] data for stomach cancer cell lines AGS, MKN1, and NUGC3. | | | |
|---|---|---|---|
| Ligand | AGS (WTp53) | MKN1 (p53$^{V143A}$) | NUGC3 (p53$^{Y220C}$) |
| **L4** | $2.7 \pm 0.2$ | $51.6 \pm 3.6$ | $2.7 \pm 0.1$ |
| **L5** | $1.6 \pm 0.06$ | $1.2 \pm 0.05$ | $1.7 \pm 0.02$ |
| **Cisplatin** | $25.0 \pm 2.4$ | $4.3 \pm 0.35$ | $20.0 \pm 1.7$ |
| **Oxaliplatin** | $7.4 \pm 0.9$ | $6.9 \pm 0.06$ | $50.0 \pm 2.7$ |
| [a] $IC_{50}$ is the concentration needed for 50% reduction of survival based on survival curves.[38] | | | |

with the data obtained at the NCI-60 screen; **L1**–**L3** displayed minimal cytotoxic activity (Table S3), whereas **L4** and **L5** were highly cytotoxic on two stomach cancer cell lines tested, AGS and NUGC3, showing a significant improvement upon $IC_{50}$ values of cisplatin and oxaliplatin. The compounds however, do not display higher in vitro cytotoxicity in NUGC3 p53-Y220C expressing cells compared to the AGS wild-type p53 cell line after 24-hours of treatment. MKN1 is insensitive to **L4** ($IC_{50}$ 51.6 μM), however, the low $IC_{50}$ value for **L5** (1.2 μM) highlights its increased cytotoxicity in comparison to the other ligands in the series.

To further characterize the anticancer potential of our lead cytotoxic compound **L5**, we assessed its cytotoxic activity in non-adherent 3D aggregate cultures of NUGC3 cells. The use of 3D cell cultures is becoming increasingly important in drug discovery due to their ability to more accurately represent physiological conditions, including cell signaling processes (cell- to cell and cell-extracellular matrix involved in cell proliferation).[39] Therefore, the use of 3D cell cultures can better predict lead compounds for in vivo testing before entering clinical trials.[40] 3D spheroids of NUGC3 cells were treated with $IC_{75}$ concentrations obtained from 2D cultures of **L5**, and compared to treatment with oxaliplatin, one of the leading drugs for gastric cancer treatment.[41] Even at the markedly lower dose of **L5** administered compared to oxaliplatin (19.5 μM vs. 250 μM at $IC_{75}$), **L5** remained more cytotoxic (Figure 6).

## Apoptotic effects of L4 and L5 in human gastric cancer cell lines

To investigate the molecular bases for the cytotoxicity of compounds **L4** and **L5**, and probe whether this mechanism is p53-dependent, we examined whether **L4** and **L5** could cleave caspase-3, an indicator of apoptosis,[42] in both AGS and NUGC3 cell lines. We also analyzed the levels of p53 expression in the cells. AGS and NUGC3 cells were treated with the indicated compounds at both $IC_{50}$ and $IC_{75}$ concentrations for 48 hours, and then cleavage of caspase-3 and p53 protein levels were assessed by Western blot. As expected, oxaliplatin induces an in-
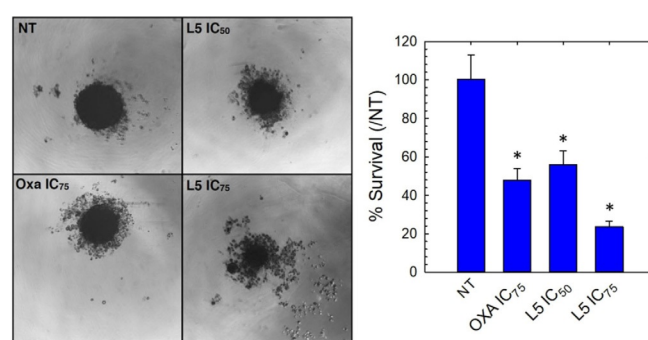
crease in p53 protein levels and low levels of cleaved caspase-3 in AGS cells are present (Figure 7).[43] Treatment with **L5** results in the presence of low caspase-3 levels comparable to oxaliplatin, again highlighting its increased cytotoxicity compared to **L4**, which does not induce any changes in either caspase-3 cleavage or p53 expression levels. In contrast to oxaliplatin, however, the increase in cleaved caspase for **L5** is not coupled with an induction of p53 protein level in the AGS (WTp53) cell line. In the NUGC3 cell line, oxaliplatin induces an increase in cleaved caspase-3 at both $IC_{50}$ and $IC_{75}$ concentrations. In addition, oligomeric forms of p53 are observed with molecular weights corresponding to dimers upon treatment with $IC_{75}$ concentrations of oxaliplatin, which could indicate p53 activation.[44] Interestingly, the level of cleaved caspase-3 upon treat-
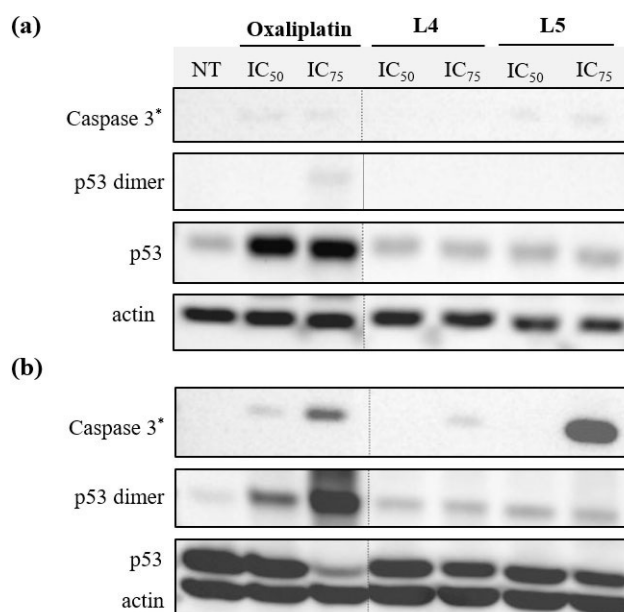


**Figure 7.** AGS cells (a) and NUGC3 cells (b) were treated for 48 hours with the $IC_{50}$ and $IC_{75}$ concentrations of indicated compound. Proteins were extracted, and 20 μg were separated on SDS PAGE. Cleaved caspase-3 (Caspase 3*), p53, and actin were then detected by Western blot analysis.

ment with **L5** at concentrations as low as 19.5 μM (IC$_{75}$ concentration) is notably increased in NUGC3 (p53-Y220C) cells in comparison to AGS (WTp53) cells under the same conditions. This suggests that the apoptotic effect of **L5** is potentiated in the Y220C mutant cell line (vide infra).

To further explore the mechanism by which **L5** imparts biological activity of p53-Y220C, we investigated whether **L5** could bind directly to the p53-Y220C mutant protein using surface plasmon resonance (SPR) (Figure S41 a). Unfortunately, binding at low micromolar concentrations was not observed, and limited solubility of **L5** beyond 400 μM prevents detection of higher micromolar affinity binding (Figure S41 B), a range relevant to a compound with the same 3,5-diiodophenol pharmacophore ($K_d = 225$ μM by ITC and $184 \pm 23$ μM by NMR).[8b] Immunoprecipitation experiments using the conformation-specific antibody Pab 240 (recognizing unfolded p53), however, showed that treatment with **L5** reduced the levels of unfolded p53, indicating that compound treatment leads to a change in conformation of mutant p53 protein (Figure S42).

### Upregulation of p53 transcriptional targets

Based on the high in vitro cytotoxicity of **L5** and its increased activity in p53-Y220C expressing cells in the cleaved caspase assay mentioned above, we further investigated the role of p53 in the biological activity of this lead compound. We measured the expression level of p53 and several p53 target genes that are involved in either cell cycle arrest (p21)[3a] or apoptosis (NOXA, PUMA)[3a, 7b] in p53-Y220C expressing and p53-silenced NUGC3 cells. p53 expression was silenced using siRNA (Figure 8). NUGC3 cells were treated for 24 hours at the IC$_{50}$ concentration and the expression level of p53 target genes were measured by RT-PCR. Upon transfection of sip53, expression levels for NOXA and p21 increase under non-treated (NT) controls compared to NT under siCT conditions. This is likely because mutant p53 can bind and inactivate p63 and p73 proteins,[45] both of which also induce cell cycle arrest and apoptosis by regulating p53 target genes such as NOXA and p21.[46] Therefore, removing mutant p53 with sip53 restores function in p63 and p73, causing their expression levels to increase. In the presence of p53-Y220C (siCT), expression levels of all three target genes was significantly higher when treated with **L5** compared to non-treated controls (NT), and are of similar levels induced by oxaliplatin, despite the lower concentration of **L5** (IC$_{50}$ **L5** = 1.7 μM vs. 50 μM for oxaliplatin) administered (Figure 8). The increase in genes PUMA and NOXA are indicative of an activation in apoptosis by **L5**, which correlates to the results obtained in Figure 7. Upon treatment with sip53, expression levels of PUMA and NOXA decrease in the case of **L5**, however, increase when treated with oxaliplatin. This is likely a result of the ability of oxaliplatin to induce apoptosis via PUMA in a p53-independent manner.[47]

Strikingly, treatment of NUGC3 cells with IC$_{50}$ values of **L5** resulted in a 4-fold increase in p21 expression compared to the non-treated control. These results are obtained without increasing p53 expression levels, unlike oxaliplatin, suggesting the restoration of wild-type function in existing p53-Y220C.
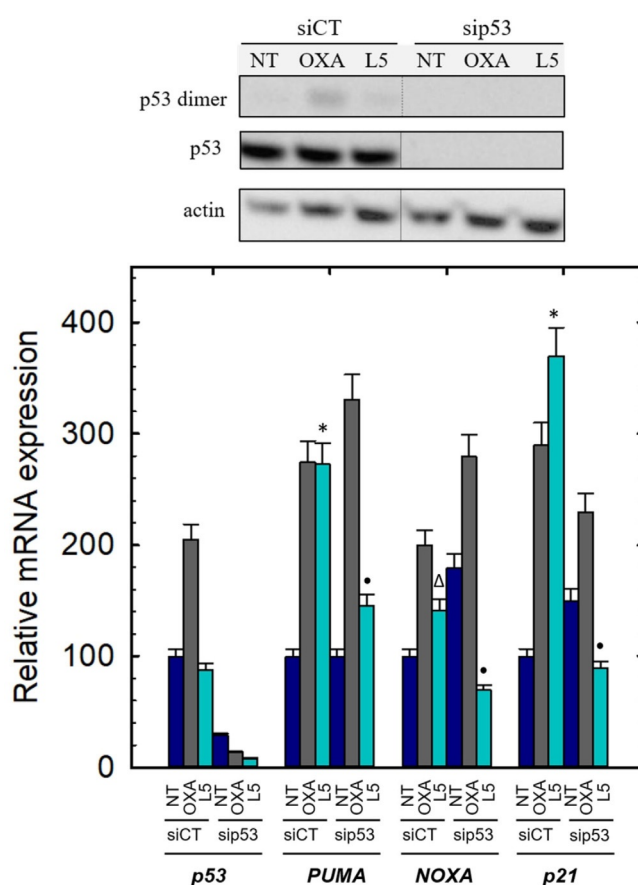


**Figure 8.** NUGC3 cells were transfected with control siRNA (siCT) or siRNA directed against p53 (sip53) and then treated for 24 hours with IC$_{50}$ concentrations of indicated compounds. Top: Proteins were extracted, and 20 μg were separated on SDS PAGE. p53 and actin were then detected by Western blotting. Bottom: Total RNAs were extracted and RT-qPCR performed to measure the expression of p53, p21, PUMA, and NOXA. Bars represent means of triplicates with error bars. * indicates statistical differences from NT (siCT) with $p < 0.001$, Δ indicates statistical differences from NT (siCT) with $p < 0.01$, ˙ indicates statistical differences from L5 (siCT) with $p < 0.001$.

Furthermore, the diminished expression of p53-Y220C upon treatment with siRNA significantly reduced the impact of **L5** on the mRNA level of the p53 target genes. These results indicate restoration of transcriptional activity to the p53-Y220C mutant, and that at least part of the biological activity of **L5** is due to restoration of wild-type p53 function.

### Summary

The pharmacological reactivation of p53 is a key target in cancer research, and there is significant promise in the development of small molecules to restore wild-type function to specific p53 mutants. In this work we have designed a series of multifunctional molecules to reactivate the common p53-Y220C mutant. We show that compounds **L4** and **L5** exhibit Zn metallochaperone activity in the Y220C mutant NUGC3 cell line. Characterization of their in vitro cytotoxicity in the NCI-60 screen and on stomach cancer cell lines AGS, MKN1, and NUGC3 identified lead compound **L5**, which displayed increased cytotoxicity compared to cisplatin and oxaliplatin. Ad-

ditionally, **L5** remained cytotoxic on 3D cell cultures, an important characteristic as these systems more directly mimic physiological conditions. Further investigation into the mechanism of action shows that **L5** induces apoptosis in the NUGC3 cell line via caspase-3, but not in AGS cells under the same conditions. This cytotoxicity is achieved at 19.5 μM, a value 10-fold larger for oxaliplatin (250 μM, $IC_{75}$). Similar reports for Y220C-dependent induction of apoptosis using small molecules have been reported at higher concentrations, albeit on shorter time scales.[8b,48] **L5** also restores p53 transcriptional activity in the p53-Y220C mutant NUGC3 cell line. Upregulation of p53 target genes PUMA, NOXA, and p21 is observed, an effect that is decreased upon knockdown of p53. These results are obtained in the absence of increased p53 expression, suggesting restoration of wild-type function.[45c] Remarkably, our results for **L5** are obtained at low doses of 1.7 μM (**L5** $IC_{50}$), demonstrating the potent activity of this scaffold.[48a,49] Although binding to recombinant p53-Y220C was not observed at such low concentrations via SPR, further structural modifications can be made to increase protein affinity and ensure further target selectivity.

Given the high level of in vitro cytotoxicity of **L5** on both p53-Y220C and WTp53 cell lines, it likely that the activity of **L5** is due to both p53-dependent and p53-independent pathways. Indeed, recent studies on p53 activating scaffolds show that increased ROS generation is an important component of the observed cytotoxicity, in addition to p53 activation.[8c,49] In the case of metal-binding agents, ROS-associated toxicity could be due to the in situ formation of redox-active Cu complexes.[8c,18a] We plan to investigate cellular levels of ROS species upon **L5** treatment both in wild-type and p53-Y220C cell lines moving forward. Overall, our novel series of bifunctional scaffolds have the potential to restore wild-type function in the p53-Y220C mutant and **L5** is a promising scaffold for future structure–activity relationship studies to increase affinity for p53-Y220C and improve selectivity. In combination with major technological advancements in gene sequencing capability and a shift towards personalized medicine, the development of small molecules capable of mutant-specific p53 reactivation holds significant promise.

## Conflict of interest

The authors declare no conflict of interest.

**Keywords:** apoptosis · cancer · drug design · metallochaperone · protein stability

[1] D. P. Lane, *Nature* **1992**, *358*, 15–16.
[2] a) T. Riley, E. Sontag, P. Chen, A. Levine, *Nat. Rev. Mol. Cell Biol.* **2008**, *9*, 402–412; b) J. T. Zilfou, S. W. Lowe, *Cold Spring Harbor Perspect. Biol.* **2009**, *1*, a001883.
[3] a) A. C. Joerger, A. R. Fersht, *Annu. Rev. Biochem.* **2016**, *85*, 375–404; b) P. A. Lazo, *Cell. Signalling* **2017**, *33*, 49–58.
[4] B. Vogelstein, D. Lane, A. J. Levine, *Nature* **2000**, *408*, 307–310.
[5] a) P. A. J. Muller, K. H. Vousden, *Nat. Cell Biol.* **2013**, *15*, 2–8; b) M. Hollstein, D. Sidransky, B. Vogelstein, C. Harris, *Science* **1991**, *253*, 49–53.
[6] M. Olivier, M. Hollstein, P. Hainaut, *Cold Spring Harbor Perspect. Biol.* **2010**, *2*, 1–17.
[7] a) J. Zawacka-Pankau, G. Selivanova, *J. Intern. Med.* **2015**, *277*, 248–259; b) K. K. Hoe, C. S. Verma, D. P. Lane, *Nat. Rev. Drug Discovery* **2014**, *13*, 217–236; c) B. Hong, A. P. J. van den Heuvel, V. V. Prabhu, S. Zhang, W. S. El-Deiry, *Curr. Drug Targets* **2014**, *15*, 80–89; d) A. Paek, J. Liu, A. Loewer, W. Forrester, G. Lahav, *Cell* **2016**, *165*, 631–642; e) G. Selivanova, K. G. Wiman, *Oncogene* **2007**, *26*, 2243–2254.
[8] a) V. J. N. Bykov, S. E. Eriksson, J. Bianchi, K. G. Wiman, *Nat. Rev. Cancer* **2017**, *18*, 89–102; b) R. Wilcken, X. Liu, M. O. Zimmermann, T. J. Rutherford, A. R. Fersht, A. C. Joerger, F. M. Boeckler, *J. Am. Chem. Soc.* **2012**, *134*, 6810–6818; c) X. Yu, A. Blanden, A. T. Tsang, S. Zaman, Y. Liu, J. Gilleran, A. F. Bencivenga, S. D. Kimball, S. N. Loh, D. R. Carpizo, *Mol. Pharmacol.* **2017**, *91*, 567–575.
[9] S. Lehmann, V. J. N. Bykov, D. Ali, O. Andrén, H. Cherif, U. Tidefelt, B. Uggla, J. Yachnin, G. Juliusson, A. Moshfegh, C. Paul, K. G. Wiman, P.-O. Andersson, *J. Clin. Oncol.* **2012**, *30*, 3633–3639.
[10] N. Mohell, J. Alfredsson, A. Fransson, M. Uustalu, S. Bystrom, J. Gullbo, A. Hallberg, V. J. N. Bykov, U. Bjorklund, K. G. Wiman, *Cell Death Dis.* **2015**, *6*, e1794–e1804.
[11] X. Peng, M. Q. Z. Zhang, F. Conserva, G. Hosny, G. Selivanova, V. J. N. Bykov, E. S. J. Arner, K. G. Wiman, *Cell Death Dis.* **2013**, *4*, e881–e887.
[12] S. N. Loh, *Metallomics* **2010**, *2*, 442–449.
[13] G. Wang, A. R. Fersht, *Proc. Natl. Acad. Sci. USA* **2012**, *109*, 13590–13595.
[14] X. Yu, A. Vazquez, A. J. Levine, D. R. Carpizo, *Cancer Cell* **2012**, *21*, 614–625.
[15] R. Puca, L. Nardinocchi, M. Porru, A. J. Simon, G. Rechavi, C. Leonetti, D. Givol, G. D'Orazi, *Cell Cycle* **2011**, *10*, 1679–1689.
[16] X. Yu, A. R. Blanden, S. Narayanan, L. Jayakumar, D. Lubin, D. Augeri, S. D. Kimball, S. N. Loh, D. R. Carpizo, *Oncotarget* **2014**, *5*, 8879–8892.
[17] C. M. Weekley, C. He, *Curr. Opin. Chem. Biol.* **2017**, *37*, 26–32.
[18] a) A. E. Stacy, D. Palanimuthu, P. V. Bernhardt, D. S. Kalinowski, P. J. Jansson, D. R. Richardson, *J. Med. Chem.* **2016**, *59*, 4965–4984; b) C. Mertens, E. A. Akam, C. Rehwald, B. Brüne, E. Tomat, M. Jung, *PLoS One* **2016**, *11*, 1–19; c) K. C. Park, L. Fouani, P. J. Jansson, D. Wooi, S. Sahni, D. J. R. Lane, D. Palanimuthu, H. C. Lok, Z. Kovacevic, M. L. H. Huang, D. S. Kalinowski, D. R. Richardson, *Metallomics* **2016**, *8*, 874–886; d) A. P. King, H. A. Gellineau, J.-E. Ahn, S. N. MacMillan, J. J. Wilson, *Inorg. Chem.* **2017**, *56*, 6609–6623; e) E. A. Akam, E. Tomat, *Bioconjugate Chem.* **2016**, *27*, 1807–1812.
[19] F. M. Boeckler, A. C. Joerger, G. Jaggi, T. J. Rutherford, D. B. Veprintsev, A. R. Fersht, *Proc. Natl. Acad. Sci. USA* **2008**, *105*, 10360–10365.
[20] a) G. D'Orazi, D. Givol, *Cell Cycle* **2012**, *11*, 2581–2582; b) R. Wilcken, G. Wang, F. M. Boeckler, A. R. Fersht, *Proc. Natl. Acad. Sci. USA* **2012**, *109*, 13584–13589.
[21] a) A. R. Fernandes, J. Jesus, P. Martins, S. Figueiredo, D. Rosa, L. M. R. D. R. S. Martins, M. L. Corvo, M. C. Carvalheiro, P. M. Costa, P. V. Baptista, *J. Controlled Release* **2017**, *245*, 52–61; b) H. Silver, Y. Chertkow, O. Weinreb, L. Danovich, M. Youdim, *Neurotherapeutics* **2009**, *6*, 86–93; c) W. J. Geldenhuys, M. B. H. Youdim, R. T. Carroll, C. J. Van der Schyf, *Prog. Neurobiol.* **2011**, *94*, 347–359; d) R. Morphy, Z. Rankovic, *J. Med.*

*Chem.* **2005**, *48*, 6523 – 6543; e) M. R. Jones, E. Mathieu, C. Dyrager, S. Faissner, Z. Vaillancourt, K. J. Korshavn, M. H. Lim, A. Ramamoorthy, V. W. Yong, T. Tsutsui, P. K. Stys, T. Storr, *Chem. Sci.* **2017**, *8*, 5636 – 5643.

[22] C. J. Van der Schyf, M. B. H. Youdim, *Neurotherapeutics* **2009**, *6*, 1 – 3.

[23] J. Fang, F. Jiang, J. Li, Y. Zhu, *Neural Regener. Res.* **2012**, *7*, 313 – 318.

[24] A. R. Blanden, X. Yu, A. J. Wolfe, J. A. Gilleran, D. J. Augeri, R. S. O'Dell, E. C. Olson, S. D. Kimball, T. J. Emge, L. Movileanu, D. R. Carpizo, S. N. Loh, *Mol. Pharmacol.* **2015**, *87*, 825 – 831.

[25] M. Frezza, S. S. Hindo, D. Tomco, M. Allard, Q. C. Cui, M. J. Heeg, D. Chen, Q. P. Dou, C. N. Verani, *Inorg. Chem.* **2009**, *48*, 5928 – 5937.

[26] A. R. Blanden, X. Yu, S. N. Loh, A. J. Levine, D. R. Carpizo, *Drug Discovery Today* **2015**, *20*, 1391 – 1397.

[27] J. S. Butler, S. N. Loh, *Biochemistry* **2003**, *42*, 2396 – 2403.

[28] A. N. Bullock, J. Henckel, B. S. DeDecker, C. M. Johnson, P. V. Nikolova, M. R. Proctor, D. P. Lane, A. R. Fersht, *Proc. Natl. Acad. Sci. USA* **1997**, *94*, 14338 – 14342.

[29] A. K. Sharma, S. T. Pavlova, J. Kim, D. Finkelstein, N. J. Hawco, N. P. Rath, J. Kim, L. M. Mirica, *J. Am. Chem. Soc.* **2012**, *134*, 6625 – 6636.

[30] a) A. E. Martell, R. D. Hancock, *Metal Complexes in Aqueous Solutions*, Springer, New York, **1996**; b) J.-S. Choi, J. J. Braymer, R. P. R. Nanga, A. Ramamoorthy, M. H. Lim, *Proc. Natl. Acad. Sci. USA* **2010**, *107*, 21990 – 21995; c) W. R. Harris, C. J. Carrano, S. R. Cooper, S. R. Sofen, A. E. Avdeef, J. V. McArdle, K. N. Raymond, *J. Am. Chem. Soc.* **1979**, *101*, 6097 – 6104.

[31] L. Alderighi, P. Gans, A. Ienco, D. Peters, A. Sabatini, A. Vacca, *Coord. Chem. Rev.* **1999**, *184*, 311 – 318.

[32] K. R. Gee, Z. L. Zhou, D. Ton-That, S. L. Sensi, J. H. Weiss, *Cell. Calcium* **2002**, *31*, 245 – 251.

[33] K. Golovine, R. G. Uzzo, P. Makhov, P. L. Crispen, D. Kunkle, V. M. Kolenko, *Prostate* **2008**, *68*, 1443 – 1449.

[34] a) J. M. Hearn, I. Romero-Canelón, B. Qamar, Z. Liu, I. Hands-Portman, P. J. Sadler, *ACS Chem. Biol.* **2013**, *8*, 1335 – 1343; b) C. Gaiddon, P. Jeannequin, P. Bischoff, M. Pfeffer, C. Sirlin, J. P. Loeffler, *J. Pharmacol. Exp. Ther.* **2005**, *315*, 1403 – 1411; c) P. Lim, A. Mahammed, Z. Okun, I. Saltsman, Z. Gross, H. B. Gray, J. Termini, *Chem. Res. Toxicol.* **2012**, *25*, 400 – 409; d) H. M. W. Verheul, D. Z. Qian, M. A. Carducci, R. Pili, *Cancer Chemother. Pharmacol.* **2007**, *60*, 329 – 339; e) O. Rixe, T. Fojo, *Clin. Cancer Res.* **2007**, *13*, 7280 – 7287.

[35] R. H. Shoemaker, *Nat. Rev. Cancer* **2006**, *6*, 813 – 823.

[36] J. Abdi, G. Chen, H. Chang, *Oncotarget* **2013**, *4*, 2186 – 2207.

[37] D. Zhang, D. Fan, *Expert Rev. Anticancer Ther.* **2007**, *7*, 1369 – 1378.

[38] J. L. Sebaugh, *Pharmaceutical Statistics* **2011**, *10*, 128 – 134.

[39] a) S. Breslin, L. O'Driscoll, *Drug Discovery Today* **2013**, *18*, 240 – 249; b) M. Zanoni, F. Piccinini, C. Arienti, A. Zamagni, S. Santi, R. Polico, A. Bevilacqua, A. Tesei, *Sci. Rep.* **2016**, *6*, 19103.

[40] a) K. M. Yamada, E. Cukierman, *Cell* **2007**, *130*, 601 – 610; b) Y. Fang, R. M. Eglen, *SLAS Discovery* **2017**, 1 – 17.

[41] a) A. Bilici, *World J. Gastroenterol.* **2014**, *20*, 3905 – 3915; b) L. Di Lauro, P. Vici, F. Belli, S. Tomao, S. I. Fattoruso, M. G. Arena, L. Pizzuti, D. Giannarelli, G. Paoletti, M. Barba, D. Sergi, M. Maugeri-Saccà, *Gastric Cancer* **2014**, *17*, 718 – 724; c) B. Chan, R. Jang, R. Wong, C. Swallow, G. Darling, E. Elimova, *Oncology* **2016**, *30*, 635 – 645; d) K. Inadomi, H. Kusaba, Y. Matsushita, R. Tanaka, K. Mitsugi, K. Arimizu, G. Hirano, A. Makiyama, H. Ohmura, K. Uchino, F. Hanamura, Y. Shibata, M. Kuwayama, T. Esaki, K. Takayoshi, S. Arita, K. Ariyama, K. Akashi, E. Baba, *Anticancer Res.* **2017**, *37*, 2663 – 2671.

[42] M. O. Hengartner, *Nature* **2000**, *407*, 770 – 776.

[43] a) H.-Y. Chen, H.-L. Cheng, Y.-H. Lee, T.-M. Yuan, S.-W. Chen, Y.-Y. Lin, P. J. Chueh, *Oncotarget.* **2017**, *8*, 15338 – 15348; b) D. Arango, A. J. Wilson, Q. Shi, G. A. Corner, M. J. Aranes, C. Nicholas, M. Lesser, J. M. Mariadason, L. H. Augenlicht, *Br. J. Cancer* **2004**, *91*, 1931 – 1946.

[44] a) G. Gaglia, Y. Guan, J. V. Shah, G. Lahav, *Proc. Natl. Acad. Sci. USA* **2013**, *110*, 15497 – 15501; b) C. D. Nicholls, K. G. McLure, M. A. Shields, P. W. K. Lee, *J. Biol. Chem.* **2002**, *277*, 12937 – 12945; c) L. T. Chong, C. D. Snow, Y. M. Rhee, V. S. Pande, *J. Mol. Biol.* **2005**, *345*, 869 – 878; d) K. Schlereth, R. Beinoraviciute-Kellner, M. K. Zeitlinger, A. C. Bretz, M. Sauer, J. P. Charles, F. Vogiatzi, E. Leich, B. Samans, M. Eilers, C. Kisker, A. Rosenwald, T. Stiewe, *Mol. Cell* **2010**, *38*, 356 – 368.

[45] a) C. Gaiddon, M. Lokshin, J. Ahn, T. Zhang, C. Prives, *Mol. Cell. Biol.* **2001**, *21*, 1874 – 1887; b) Y. Li, C. Prives, *Oncogene* **2007**, *26*, 2220 – 2225; c) P. Muller, K. Vousden, *Cancer Cell* **2014**, *25*, 304 – 317.

[46] E. C. Pietsch, S. M. Sykes, S. B. McMahon, M. E. Murphy, *Oncogene* **2008**, *27*, 6507 – 6521.

[47] X. Wang, M. Li, J. Wang, C.-M. Yeung, H. Zhang, H.-f. Kung, B. Jiang, M. C.-M. Lin, *Biochem. Pharmacol.* **2006**, *71*, 1540 – 1550.

[48] a) X. Liu, R. Wilcken, A. C. Joerger, I. S. Chuckowree, J. Amin, J. Spencer, A. R. Fersht, *Nucleic Acids Res.* **2013**, *41*, 6034 – 6044; b) in Similar reports by Fersht and co-workers show p53 Y220C-depedent induction of caspase-3 at 200 μm for PK7088, however, at an earlier time point of 6 hours (see Ref. [44a]). Boeckler and co-worker also report NUGC3-depedent induction of apoptosis after 6 hours, at concentrations of 50 and 100 μm for PhiKan5196 and PhiKan5974 respectively (Ref. [8b]). Vol..

[49] M. R. Bauer, A. C. Joerger, A. R. Fersht, *Proc. Natl. Acad. Sci. USA* **2016**, *113*, E5271 – E5280.